ACS Chemical Neuroscience

Letter

pubs.acs.org/chemneuro

Novel Hexapeptide Interacts with Tubulin and Microtubules, Inhibits Aβ Fibrillation, and Shows Significant Neuroprotection

Atanu Biswas,[†] Prashant Kurkute,[†] Suraiya Saleem,[‡] Batakrishna Jana,[†] Saswat Mohapatra,[†] Prasenjit Mondal,[†] Anindyasundar Adak,[†] Subhajit Ghosh,[†] Abhijit Saha,[†] Debmalya Bhunia,[†] Subhash Chandra Biswas,[‡] and Surajit Ghosh*[,†,§]

[†]Organic and Medicinal Chemistry Division, CSIR-Indian Institute of Chemical Biology Campus, 4 Raja S. C. Mullick Road, Kolkata 700 032, India

[‡]Cell Biology and Physiology Division, CSIR-Indian Institute of Chemical Biology, 4 Raja S. C. Mullick Road, Jadavpur, Kolkata 700 032, West Bengal India

[§]Academy of Scientific and Innovative Research (AcSIR), CSIR-Indian Institute of Chemical Biology Campus, 4 Raja S. C. Mullick Road, Kolkata 700 032, India

Supporting Information

ABSTRACT: Herein, we report a novel hexapeptide, derived from activity dependent neuroprotective protein (ADNP), that spontaneously self-assembles to form antiparallel β-sheet structure and produces nanovesicles under physiological conditions. This peptide not only strongly binds with β-tubulin in the taxol binding site but also binds with the microtubule lattice *in vitro* as well as in intracellular microtubule networks. Interestingly, it shows inhibition of amyloid fibril formation upon co-incubation with Aβ peptide following an interesting mechanistic pathway and excellent neuroprotection in PC12 cells treated with anti-nerve growth factor (NGF). The potential of this hexapeptide opens up a new paradigm in design and development of novel therapeutics for AD.

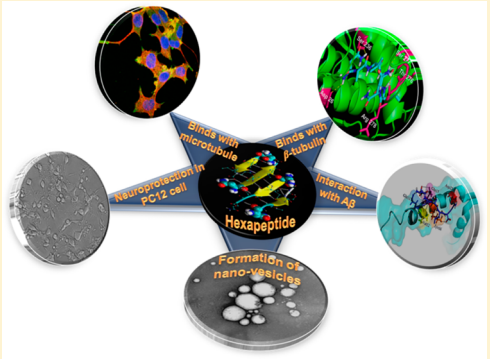

KEYWORDS: *Aβ42 peptide, neuroprotective peptide, tubulin, microtubule, PC12 cell*

In the last three decades, Alzheimer's disease (AD) has become a major threat for elderly people around the globe, and millions of people are suffering with this devastating disease.[1] Amyloid-β (Aβ) peptide plays a central role in AD, misfolds into the β-sheet rich conformation, forms long unbranched fibers, and becomes insoluble inside the cellular milieu, depositing as amyloid plaques followed by disruption of neuronal networks.[2−4] Aβ fiber is also known to disrupt intracellular microtubule networks.[5,6] Therefore, development of a novel inhibitor for Aβ fibrillizations is extremely important for potential therapy of AD. To date, there are no approved therapies for inhibiting amyloid fibrillizations. However, many small molecules, including one octapeptide (**NQ**, NAPVSIPQ) inhibit fibrillizations *in vitro*.[7−13] Among them, the small molecule clioquinol inhibits *in vivo* Aβ fibrillizations, and **NQ** inhibits *in vivo* tau hyperphosphorylation.[4] Interestingly, the Shoichet group and others have found that many fibrillization inhibitor-like molecules form spontaneous chemical aggregates, which are colloidal-like particles with varying sizes from 50 to 600 nm.[14] Recently, we have also found that **NQ**, which is known to inhibit tau hyperphosphorylation *in vivo*, spontaneously forms amyloid-like fibrils and inhibits amyloid fibril formation *in vitro*.[13] Although there are a few molecules, like clioquinol and **NQ**, that inhibit Aβ fibrillizations and show potential in *in vivo* studies, the success rate in clinical stages is still poor. Therefore, development of a potential amyloid inhibitor is extremely important for the treatment of AD. In this paper, for the first time, we have designed a novel short hexapeptide that is spontaneously self-assembled and forms nanovesicles, interacts with tubulin and microtubules close to the taxol binding site, inhibits amyloid fibrillizations *in vitro*, and provides excellent protection against NGF deprivation induced neuronal cell death.

We have designed this novel hexapeptide, Asn-Ala-Val-Ser-Ile-Gln (**NV**, Figure 1a) from activity dependent neuroprotective protein (ADNP) and synthesized this peptide as well as its biotin and FITC-tagged forms in our laboratory through solid phase peptide synthesis methods followed by purification through HPLC (Figure S1−S4, Supporting Information) and characterization by mass spectrometry. First, we have checked the self-assembly behavior of **NV** by molecular dynamics (MD) simulation. MD simulation of **NV** reveals atomic detail and the nature of self-assembly in solution.

Received: May 27, 2015
Accepted: July 6, 2015
Published: July 6, 2015

DOI: 10.1021/acschemneuro.5b00149
ACS Chem. Neurosci. 2015, 6, 1309−1316

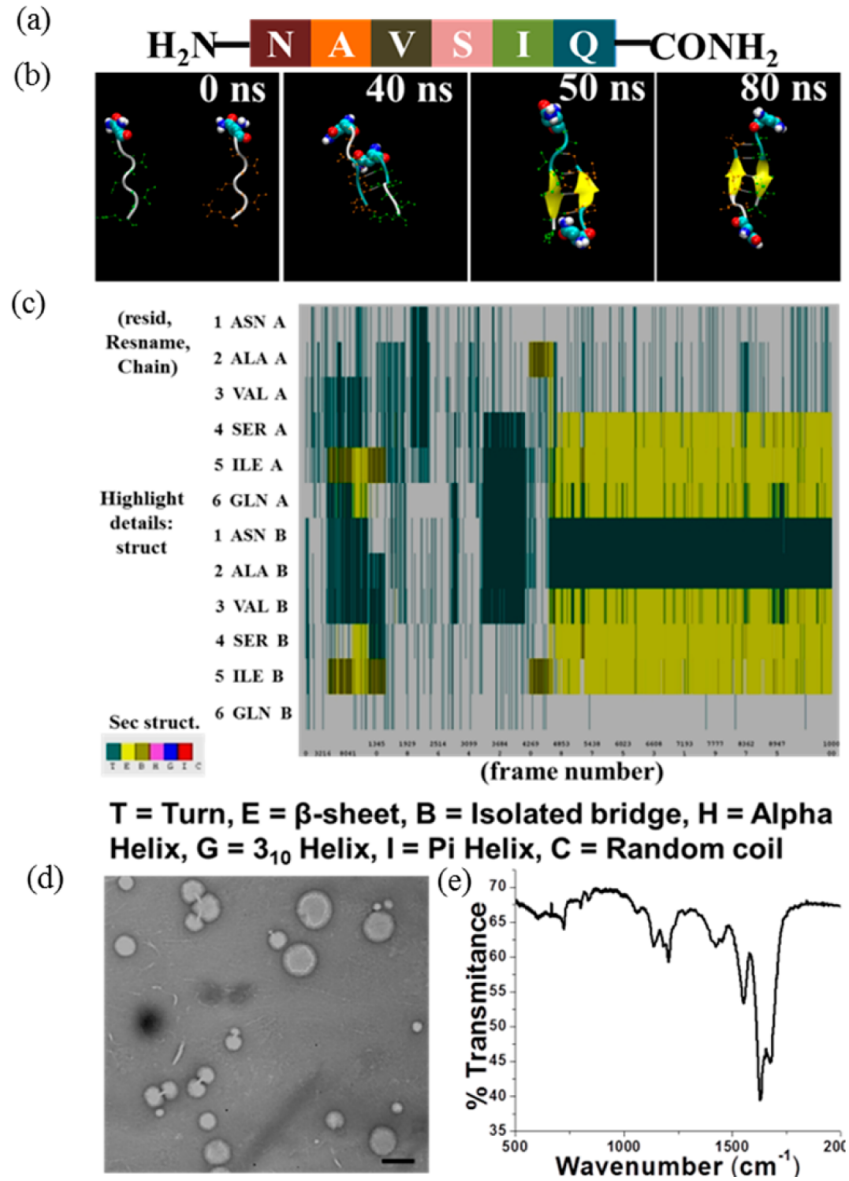

Figure 1. (a) Amino acid sequence of **NV**. (b) Snapshots from a MD simulation movie of **NV** demonstrating how it assembles rapidly to antiparallel β-sheet structure. (c) Secondary structure with the change of time reveals that alanine, valine, serine, isoleucine, and glutamine of **NV** are involved in antiparallel β-sheet structure formation. (d) **NV** self-assembles to form nanovesicles (Scale bar corresponds to 100 nm). (e) FT-IR spectrum of 1 h incubated sample of **NV** reveals β-sheet structure.

Initially, both two and four molecules of **NV**, denoted as orange (**O**) and green (**G**), were separated by 2 nm in the simulation box and simulated for 100 ns. We found that the interactions between the **NV**s are dynamic in the initial stage of simulation (Figure 1b). After simulation up to 20 ns, **O** and **G** peptides start interacting with each other in parallel orientation (Figure 1b and Supporting Information Figure S5). After 40 ns of simulation, β-turn rich structure was observed through H-bonding interactions between serine, isoleucine, and glutamine of **O** chain and alanine, valine, and serine of **G** chain, respectively (Figure 1b and Supporting Information Figure S5). Interestingly, at 50 ns, they form antiparallel β-sheet-like structure through strong H-bonding interactions between glutamine, isoleucine, serine, and valine of chain **O** and alanine, valine, serine and isoleucine of chain **G**, respectively (Figure 1b and Supporting Information Figure S5). After 80 ns, stable β-sheet structure was formed due to H-bonding interactions between valine, serine, isoleucine, and glutamine of chain **O** and isoleucine, serine, valine, and alanine of chain **G**, respectively (Figure 1b and Supporting Information Figure S5). The energy diagram confirms the stability of this β-sheet structure up to 100 ns (yellow color region of Figure 1c) simulation of **NV**. We have found from the simulation that five key amino acids, alanine, valine, serine, isoleucine, and glutamine, in the hexapeptide backbone are responsible for the formation of this β-sheet structure (Figure 1c). From the MD simulation movies, we envision that the assembly process starts from the β-turn like structure and rapidly converts to the β-sheet rich (Figure 1b and Supporting Information Figure S5 and Movies S1 and S2). This result motivated us to explore the self-assembly behavior of **NV** by various experimental techniques. First, we performed the FT-IR spectroscopic studies of 1 h incubated sample of **NV**, which clearly shows β-sheet conformation as we observed a high absorption peak at

DOI: 10.1021/acschemneuro.5b00149
ACS Chem. Neurosci. 2015, 6, 1309−1316

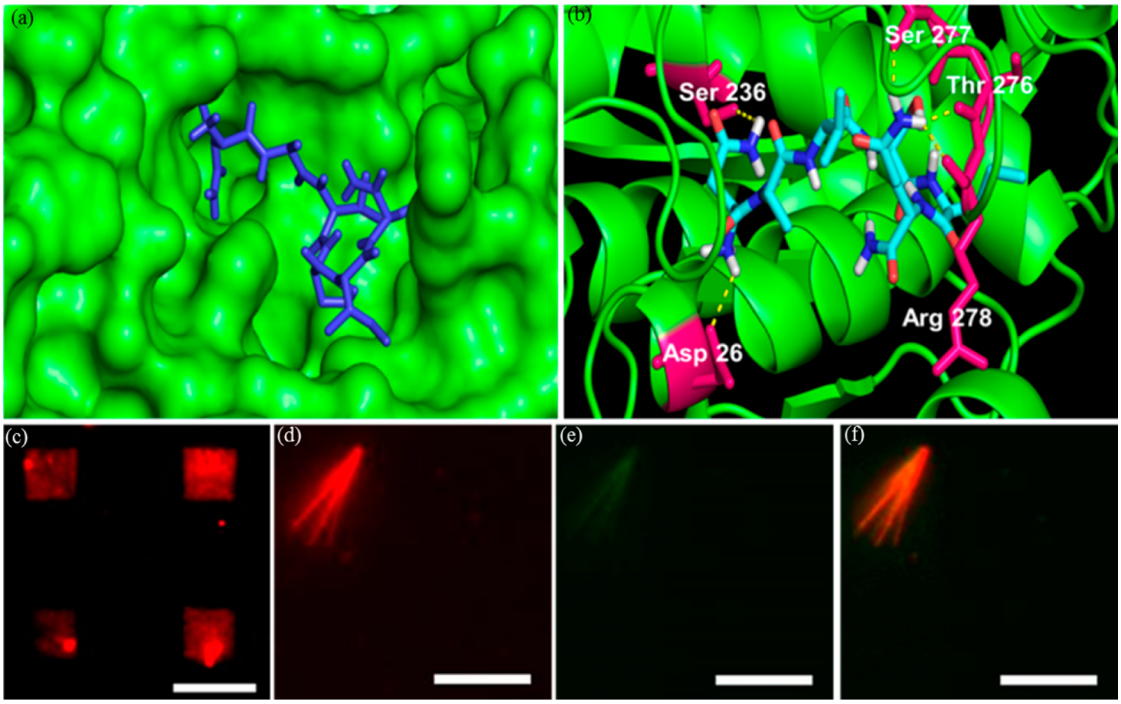

Figure 2. (a) Docking image reveals the interaction of **NV** with β-tubulin through hydrophobic interaction. (b) Specific interaction between the amino acids of β-tubulin and **NV**. (c) Microscopic image reveals that the tubulin specifically binds with **NV**, immobilized on biotin micropatterned surfaces. (d) Red colored microtubules represent alexa-568 labeled polymerized microtubules. (e) Green colored microtubules represent that **FITC-NV** binds with polymerized microtubules. (f) Merged image confirms the binding of **FITC-NV** with polymerized microtubules. Scale bar corresponds to 10 μm.

1628 cm^{-1} in the amide I region, which is the signature peak for β-sheet conformation (Figure 1e).[13] The β-sheet conformation of **NV** in the solution was further confirmed by circular dichroism (CD), as we observed negative ellipticity at 219 nm, which is the signature peak of β-sheet conformation (Supporting Information Figure S6). Therefore, the MD simulation result corroborates the FT-IR result, and the CD data clearly indicates that **NV** spontaneously self-assembles in solution. These results further motivated us to study the morphology of **NV** using transmission electron microscopy (TEM). Time-dependent TEM images of 100 nM **NV** at 37 °C reveal an extremely interesting process of self-assembly, which leads to the formation of nanovesicles (Figure 1d). The TEM image of day 1 reveals 10−40 nm width fibrils, while in day 2, fibrillar structures further self-assemble and form coiled nest-like structure, and finally in day 3, further self-assembly results in the formation of nanovesicles (Supporting Information Figure S7). In AD, microtubules are disrupted, which affects cytoskeleton organization; thus protecting microtubules from disruption by small molecules is extremely important. Therefore, we became interested to investigate whether **NV** can provide stability in the microtubule lattice through binding with microtubules. Initially, we have tried to find out the exact binding site of **NV** in tubulin by docking. Docking results indicate that **NV** is binding with β-tubulin near the taxol binding site through hydrophobic interaction and H-bonding interaction, which is important for microtubule stability (Figure 2a and Supporting Information Figure S8). From docking results, we have also found the binding partners (amino acids) between **NV** and tubulin as follows: asparagine (amide and amine group) of **NV** is H-bonded with two amino acids of tubulin, one of them is Ser236 (−OH group) and the other one is Asp26 (−COOH group). On the other hand, glutamine (amide group) of **NV** is H-bonded to Thr276 (−OH group) and the −C═O groups of both Ser277 and Arg278 of β-tubulin (Figure 2b and Supporting Information Figure S8). In addition, docking results show that **NV** adopts a bent structure on the tubulin surface (Figure 2b and Supporting Information Figure S9). The binding of **NV** to the taxol binding site was further confirmed by tubulin turbidity assay[15] and microtubule polymerization assay.[16] It was found that **NV** promotes the tubulin polymerization because the rate of increase of tubulin turbidity in the presence of **NV** is higher than the control (Supporting Information Figure S10a) and also the rate of increment of DAPI fluorescence is also higher in the presence of **NV** compared with control (Supporting Information Figure S10b). These two results also support the binding of **NV** to the taxol binding site of tubulin because it is known that drugs that bind to the taxol binding site of tubulin among four major binding sites (taxol, colchicine, vinblastine, and GTP) induce tubulin polymerization.[17−19] As a result, there is increase in tubulin turbidity and the rate of microtubule assembly. In the other three cases, tubulin turbidity decreases. We further determined the binding constant of the **NV** to the tubulin by a fluorescence intensity quenching study of the intrinsic tryptophan residue of tubulin.[19] The binding constant was found to be 1.14×10^3 M^{-1} (Supporting Information Figure S11). These results further motivated us to study this binding through our previously developed *in vitro* assay based on chemically modified micropatterned surface chemistry. In brief, we have used our recently developed biotin micropatterned surface and immobilized freshly prepared biotinylated-**NV** (**Biotin-NV**) onto the micropattern through neutravidin followed by incubation with tubulin mix (80:20 unlabeled tubulin and Alexa568 labeled tubulin) in the presence of GTP at 37 °C and observed using a TIRF microscope. After 30 min

DOI: 10.1021/acschemneuro.5b00149
ACS Chem. Neurosci. 2015, 6, 1309−1316

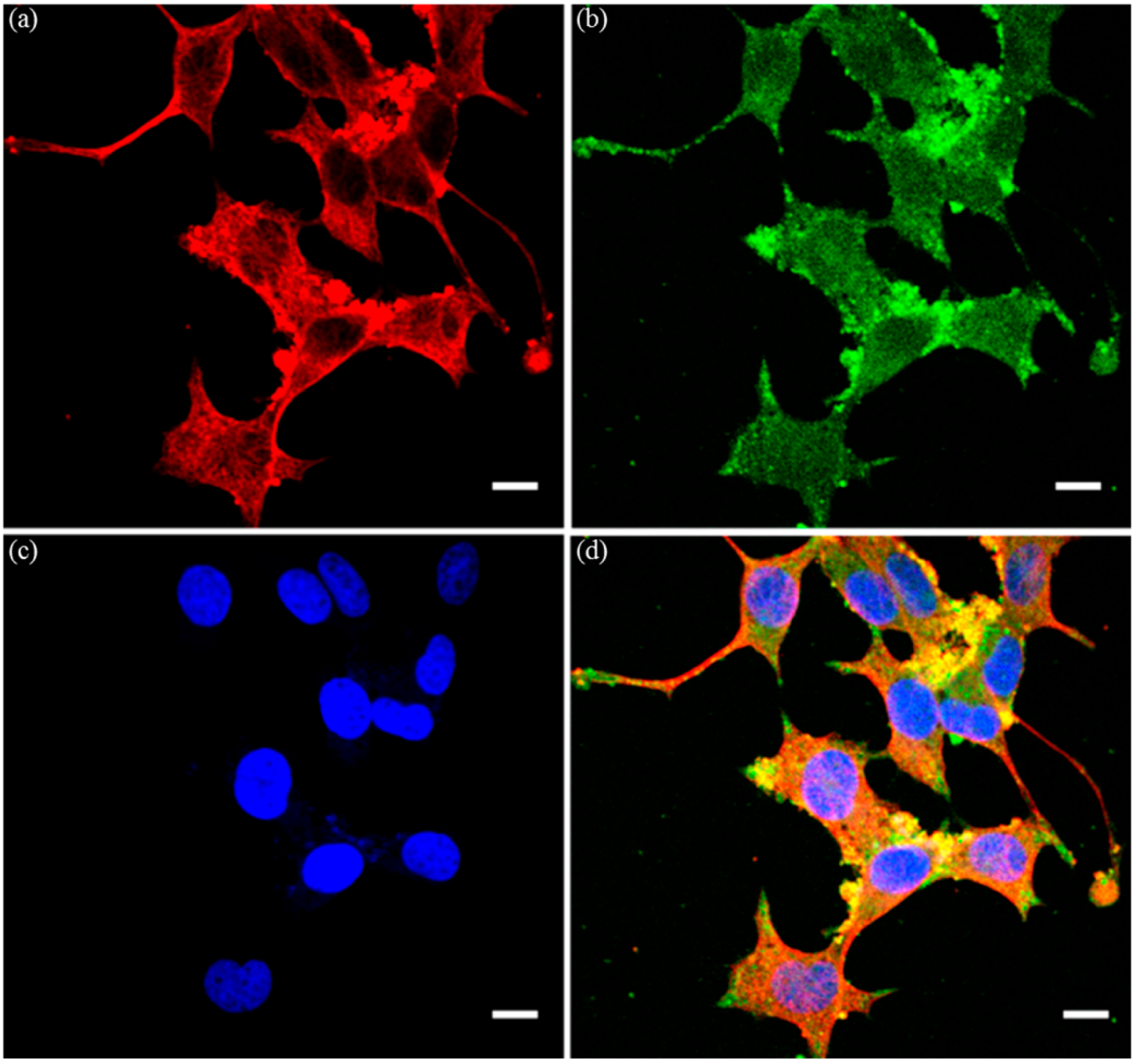

Figure 3. Confocal images reveal binding of **NV** with intracellular tubulin/microtubule networks of PC12 cells. (a) Red colored microtubule networks of PC12 cells at 561 nm channel; (b) green tiny particles are distributed along the microtubule networks and all over the PC12 cells at 488 nm channel; (c) blue colored nucleus of PC12 cells at 405 nm channel; (d) Yellow colored merged image reveals that **NV** binds along the intracellular microtubules of PC12 Cells. Scale bar corresponds to 30 μm.

incubation at 37 °C, we observed localized binding of tubulin with **Biotin-NV** immobilized biotin micropatterns as we observed red colored micropatterns in the 561 nm channel (Figure 2c). A control experiment was performed in the absence of the peptide, following a similar method as described, which resulted in no tubulin binding on the micropattern (data not shown).[13] Next, we have checked whether **NV** binds with polymerized tubulin. Here, we have used FITC-labeled **NV** (**FITC-NV**) during polymerization of Alexa568 labeled tubulin *in vitro* in the presence of GTP following the previously described tubulin polymerization method and visualized polymerized microtubules using a TIRF microscope. Microscopic images reveal a green colored microtubule bundle under the 488 nm laser (Figure 2e), red colored microtubules under the 561 nm laser (Figure 2d), and yellow colored microtubules in the merged channel (Figure 2f). This data clearly indicates that **NV** not only interacts with tubulin but also interacts with microtubules and does not perturb microtubule polymerization.

We have found that **NV** interacts with tubulin and microtubules from *in vitro* study, which further motivated us to investigate whether **NV** interacts with intracellular tubulin and microtubules. For that purpose, we have performed a microtubule colocalization study using confocal microscope. We have incubated **FITC-NV** with 3000−5000 cell densities of rat neuronal PC12 cells for 16 h. Cells were washed and fixed with 4% paraformaldehyde and permeabilized with 0.2% triton-X. Then cellular microtubules were visualized as red color using primary polyclonal anti-α-tubulin antibody and fluorescent tagged secondary antibody. Nucleus was stained with Hoechst 33258. Interestingly, from confocal images, we have found yellow colored colocalized images inside the PC12 cells (Figure 3d), which clearly indicates the colocalization of FITC-labeled green colored peptide (Figure 3b) and red colored microtubule

DOI: 10.1021/acschemneuro.5b00149
ACS Chem. Neurosci. 2015, 6, 1309−1316

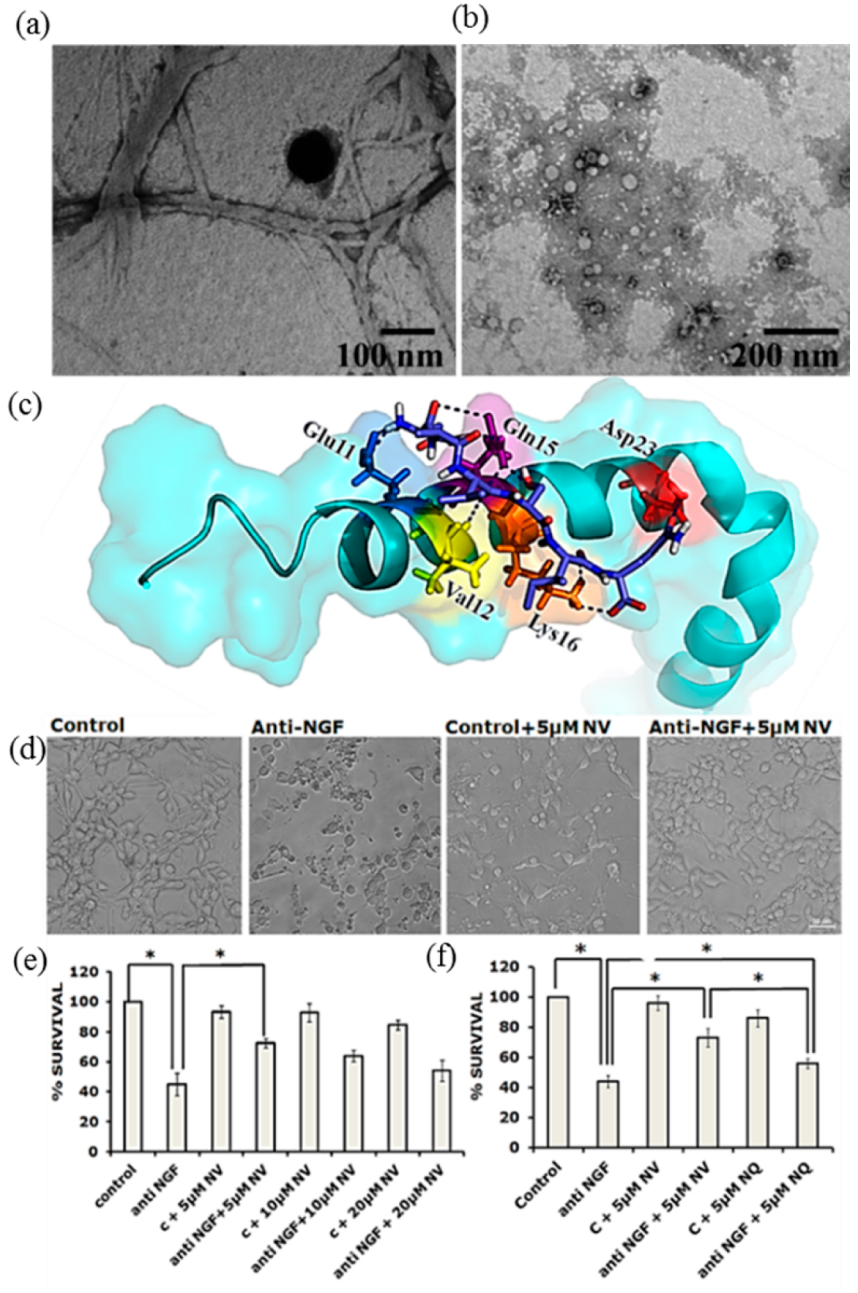

Figure 4. TEM image reveals the inhibition of Aβ fibrillization. (a) Aβ peptide (100 nM) forms fiber after 7 days incubation at 37 °C in PBS buffer; (b) 7 day co-incubated sample of 100 nM Aβ peptide and 100 nM **NV** in PBS buffer at 37 °C shows nanovesicles with very short fibril-like structure; (c) **NV** interacts with Aβ peptide and its interacting partners; (d) inhibitor **NV** protects neuronally differentiated PC12 cells against NGF deprivation. Neuronally differentiated PC12 cells were treated with anti-NGF in presence and absence of different doses of inhibitor **NV** for 20 h. Representative images show increased survival with retention of neuronal processes in PC12 cells treated with anti-NGF in the presence of 5 μM NV. (e) Graphical representation of percentage of cell survival after anti-NGF treatment in the presence of 5, 10, and 20 μM **NV**. (f) Inhibitor **NV** provides higher protection than inhibitor **NQ.** Graphical representation of percentage of cell viability following anti-NGF treatment in the presence of 5 μM **NV** and 5 μM **NQ.** Data represented as mean ± SEM of three independent experiments performed in triplicate. The asterisk denotes statistically significant differences between indicated classes: *$p < 0.05$. Scale bar corresponds to 30 μm.

networks in PC12 cells (Figure 3a). Figure 3c represents the nucleus of PC12 cells, stained by Hoechst. Therefore, these results clearly indicate that **NV** binds with intracellular tubulin and microtubules.

Next, we have checked whether this peptide has an inhibitory effect against Aβ fibrillization because this peptide was designed from ADNP. Initially, we used TEM to understand the inhibition of Aβ fibrillizations. For that purpose, we co-incubated Aβ42 peptide and **NV** for 7 days. After 7 days incubation, TEM images reveal nanovesicular structures with sporadic very short disrupted fiber-like structure (Figure 4b), while Aβ peptide alone under similar conditions forms fibrils (Figure 4a). This data clearly indicates that **NV** inhibits amyloid fibrillizations *in vitro*. Since **NV** inhibits the fibril formation of Aβ peptide, we became interested to determine how **NV** interacts with Aβ peptide using molecular docking. Docking study reveals that **NV** interacts with Aβ (PDB ID 1IYT)[20] through hydrophobic interaction and H-bonding interaction.

DOI: 10.1021/acschemneuro.5b00149
ACS Chem. Neurosci. 2015, 6, 1309−1316

We have also found that the H-bonding helps in the interaction between the side chain of asparagine ($-NH_2$) of **NV** and $-C{=}O$ group of Glu11. Further, the $-C{=}O$ groups of alanine, valine, isoleucine, and glutamine interact with the $-NH_2$ group of Gln15, the $-OH$ group of Val12, the $-NH_2$ group of Lys16, and the $-OH$ group of Asp23, respectively (Figure 4c and Supporting Information Figure S12). It was described before that Aβ fibril formation occurs through antiparallel interaction of one Aβ monomer with the adjacent Aβ peptide through the hydrophobic stretch of residues 17−21 of the Aβ molecule.[21] Further, it was shown that Aβ peptide inhibitors bind to the hydrophobic stretch of residues 17−21;[22−24] thus Aβ fibril formation can be prevented by inhibiting incoming Aβ molecule through blocking this site.[2−4] In our docking experiment, we have also found that **NV** binds to the hydrophobic region of residues 11−23 of Aβ. Therefore, the Aβ peptide fibril is inhibited due to blocking of the site by **NV**. However, much detailed study is needed to confirm the binding of **NV** to Aβ and the mechanism of inhibition of Aβ fibrillation by **NV**.

This data further motivated us to investigate whether **NV** exhibits neuroprotection against anti-NGF toxicity. It has been shown before that withdrawal of NGF from differentiated PC12 cells led to overproduction of Aβ peptide.[25] Neuronal cell death and Aβ production in differentiated PC12 cells in response to NGF deprivation was completely blocked by inhibition of Aβ processing by β- and γ-secretase inhibitors or antibodies directed against Aβ peptide.[25] Moreover, experimental studies in NGF deficient transgenic mice and mechanistic studies on the antiamyloidogenic action of NGF signaling in primary cultures of neuronal cells revealed a fundamental link between NGF signaling deficiency and Alzheimer's neurodegeneration.[26] Thus, we studied the neuroprotective potential of the inhibitor **NV** in neuronal cell line PC12.[27] These cells were differentiated in NGF containing medium for 5 days. On the fifth day they were treated overnight with anti-NGF along with different doses of inhibitor **NV** (Figure 4d). NGF deprivation results in death of PC12 cells, and it has been widely used to study the mechanism of death of neurons.[28,29] Hence, this model is employed for assessing the neuroprotective potential of the inhibitor. The cells were observed under the microscope on the day following treatment; survival was assessed by intact nuclear counting assay (Figure 4d). The results suggested that the inhibitor **NV** provided protection to the cells compared with cells subjected to NGF withdrawal. However, at higher concentrations, it did not provide better protection and showed toxicity to control cells. **NV** (5 μM) showed significant protection to cells compared with 10 and 20 μM (Figure 4e). Importantly, cells maintained in the presence of 5 μM **NV** also retained overall neuronal morphology including neuronal processes even after NGF deprivation. Further, it was observed that inhibitor **NV** provided better protection to neuronal PC12 cells than **NQ** (positive control), to death induced by NGF deprivation (Figure 4f).

In summary, we have demonstrated that a novel hexapeptide spontaneously self-assembles to form nanovesicles and inhibits the Aβ fibrillizations *in vitro*. In addition, this novel peptide binds with tubulin and microtubules close to the taxol binding site and exhibits excellent neuroprotection against in neuronal cell line. To the best of our knowledge this is the shortest peptide that served as an excellent inhibitor for Aβ fibrillizations and as an excellent neuroprotector. We also observed that neuroprotection by **NV** follows a similar pathway to that recently proposed by the Shoichet group.[11]

METHODS

Reagents. All the Fmoc-amino acids, 2-(1*H*-benzotriazol-1-yl)-1,1,3,3-tetramethyluronium hexafluorophosphate (HBTU), and Rink Amide AM resin were purchased from Novabiochem. D-Biotin was purchased from Thermo Fisher. Piperidine, diisopropylethylamine (DIPEA), and 1-hydroxybenzotriazole (HOBT) anhydrous were purchased from Spectrochem. Phenol, dichloromethane (DCM), ethanedithiol (EDT), thioflavine-T, trifluoroacetic acid, hydrogen peroxide (30% solution), acetone, dichloromethane, and *N*,*N*′-dimethylformamide were purchased from Merck. 3-Glycidoxypropyl-trimethoxysilane, *N*,*N*′-diisopropylcarbodiimide (DIC), nickel(II) chloride hexahydrate, 5(6)-carboxyfluorescein, Amberlite-IRA400, guanosine 5′-triphosphate sodium salt hydrate (GTP), 4,6-Diamidino-2-phenylindole (DAPI), and cell cultured DMSO were purchased from Sigma-Aldrich. Diamino-poly(ethylene glycol) with MW3000 Da (NH_2-PEG_{3000}-NH_2) was purchased from Rapp Polymere. E,Z-Link biotin-NHS was purchased from Pierce. Human recombinant NGF was purchased from Sigma (St. Louis, MO, USA). Culture medium and serum were purchased from Invitrogen. Pyridine and ether were purchased from Fisher Scientific. For purification, we use Shimadzu HPLC system with Symmetry C-18 (Waters) semi-preparative reverse phase column. Vertis 4K freeze drier was used to lyophilize the pure product after column purification. HPLC grade water and acetonitrile were purchased from J. T. Baker.

Tubulin. Tubulin was isolated from goat brain. The purification of tubulin from goat brain and its labeling were performed as described in the literature (Supporting Information).

Peptide Synthesis. Hexapeptide **NV** (NH_2-NAVSIQ-NH_2), biotin-hexapeptide **Biotin-NV** (biotin-NAPVSIPQ-NH_2), **FITC-NV** (FITC-NAVSIQ-NH_2), and octapeptide **NQ** (NH_2-NAPVSIPQ-NH_2) have been synthesized by solid phase peptide synthesis methods using Rink Amide AM resin in a CEM microwave peptide synthesizer. Crude peptides were purified by HPLC (Shimadzu) and characterized by MALDI mass spectrometry.

Transmission Electron Microscopy (TEM). A 10 μL aliquot of the 100 nM solution of **NV** was incubated at 37 °C. After 1, 2, and 3 days, the incubated solutions were placed on a 300 mesh copper grid from ProSciTech. After 1 min, excess solution was removed, and the grid was washed with water followed by staining with 2% uranyl acetate in water. Samples were viewed using a TECNAI G2 SPIRIT BIOTWIN CZECH REPUBLIC 120 kV electron microscope operating at 80 kV.

Fourier Transform Infrared Spectroscopy. The freshly prepared peptide was incubated for 1 h and lyophilized, and FT-IR spectroscopic analysis was carried out in a PerkinElmer Spectrum 100 FT-IR spectrometer using KBr pellets. Spectra of these pellets were recorded and accumulated from 5 times scan with speed 0.2 cm/s at a resolution of 1.6 cm^{-1} in a PerkinElmer Spectrum 100 series spectrometer. The $LiTaO_3$ detector was used for data plotting. Each time, background correction was performed to eliminate interference from air (or any other parameters).

Circular Dichroism (CD). CD was performed on a JASCO (J-810) spectrometer to study the conformation of **NV** in solution. A 100 μM solution of **NV** in Milli-Q water was used for the CD study, and the data was analyzed in origin Pro 8.5 software.

Tubulin Turbidity Assay. We have performed tubulin turbidity assays in the presence of GTP. Tubulin (20 μM), 4 mM GTP, 10% dimethyl sulfoxide, and 100 μM **NV** were mixed in Brinkley Reassembly Buffer 80 (BRB 80) in ice and injected into 37 °C heated quartz cuvettes of path length 10 mm. The turbidity was measured by measuring absorbance of the solution at 350 nm for 40 min in the UV−vis spectrophotometer (G6860A Cary 60 UV−vis spectrophotometer, Agilent Technologies). DMSO was used to initiate the polymerization. The control experiment was carried out following the same procedure in the absence of **NV**.

DOI: 10.1021/acschemneuro.5b00149
ACS Chem. Neurosci. 2015, 6, 1309−1316

Microtubule Assembly Assay. The assay was carried out following a previously described procedure. In brief, a mixture of 10 μM DAPI in BRB80 buffer containing 100 μM tubulin, 10 mM GTP, and 100 μM **NV** was prepared. The solution was excited at 355 nm wavelength at 37 °C, and the emission spectrum of the solution was recorded in the region from 400 to 600 nm wavelength for 60 min in 5 min time intervals in a Quanta Master spectrofluorometer (QM-40), which is equipped with Peltier module for controlling the temperature during experiment. A control experiment was carried out under same condition in the absence of **NV**. The data was calculated in origin Pro 8.5 software.

Determination of Binding Affinity of NV with Tubulin by Fluorescence Intensity Quenching Study of the Intrinsic Tryptophan Residue of Tubulin. Drugs that bind to the tubulin quench the intrinsic tryptophan fluorescence intensity of tubulin. So, the intrinsic tryptophan fluorescence intensity of tubulin was measured in the presence of different concentrations of **NV**. From that, a binding constant was calculated using a modified Stern−Volmer equation. Tubulin (10 μM) was mixed with different concentrations of **NV** in BRB80 buffer in ice, and the fluorescence emission spectra were recorded from 310 to 450 nm after excitation of the sample at 295 nm at 4 °C in Quanta Master spectrofluorometer (QM-40) equipped with a Peltier module for controlling the temperature.

Hexapeptide NV Binding with Microtubules at Tubulin Polymerization. *Mixture 1.* Alexa Fluor 568-labeled tubulin (0.5 μL, 15 mg mL^{-1}, 65% labeling ratio), tubulin (2 μL, 20 mg mL^{-1}), **FITC-NV** (0.5 μL, 1 mM), GTP (0.2 μL, 1 mM), and BRB80 (1.8 μL; 80 mM PIPES, 1 mM EGTA, 1 mM $MgCl_2$, pH adjusted to 6.8 by using concentrated KOH solution) were mixed on ice. The mixture was incubated for 30 min in a 37 °C water bath.

Mixture 2. Taxol (0.4 μL, 1 mM) and BRB80 (180 μL) were mixed.

Final Mixture. After 30 min incubation, 40 μL of warmed mixture **2** was added into mixture **1**. Then this mixture was separated in a table top centrifuge (7 min, 12000 rpm, Eppendorf 5810R benchtop centrifuge, rotor type F-34−6−38). The colored pellet was resuspended in warm mixture **2**.

Ten microliters of resuspended solution of microtubule was placed on a glass coverslip and imaged under an inverted fluorescence microscope (NIKON Ti−U) at 40× magnification using an ANDOR iXON3 camera.

Hexapeptide NV and Aβ42 Interaction. A 100 nM solution of Aβ42 alone and mixture of Aβ42 (final concentration 100 nM) and **NV** (final concentration 100 nM) were incubated differently for 7 days. After 7 days, both solutions were deposited on carbon coated TEM grids, and the morphology was studied under transmission electron microscope.

Hexapeptide NV−Tubulin Interaction Study on Biotin Micropatterned Surface. Biotin micropatterned surfaces were prepared by a previously described method. A flow chamber of around 5 μL was built from one biotin-patterned glass surface and one poly(L-lysine) (PLL)−PEG passivated counter glass, separated by two strips of double sticky tape (Tesa). The flow chamber was equilibrated with BRB80 and incubated with β-casein for 10 min followed by washing with 20 μL of BRB80 for complete removal of unbound β-casein. Neutravidin (100 nM) was flowed into the flow chamber and incubated for 10 min followed by removal of excess neutravidin with 20 μL of BRB80. Biotinylated-hexapeptide (**Bio-NV**, 1 mM) in BRB80 was flowed into the flow chamber and incubated for 10 min, and unbound peptide was washed away by 20 μL of BRB80. Then, the flow chamber was filled with 18.5 μM tubulin mix (80:20 unlabeled tubulin and Alexa568 tubulin) in BRB80 supplemented with 3 mM GTP, 10 mM $MgCl_2$, and an oxygen scavenger system (50 mM glucose, 1 mg mL^{-1} glucose oxidase, and 0.5 mg mL^{-1} catalase) on an ice cold metal block and placed in the TIRF microscope at 37 °C. The flow chamber was imaged using an IX-81 total internal reflection fluorescence (TIRF) microscope (Olympus) with a 60× TIRFM objective (Olympus; Hamburg, Germany) and an Andor iXon3 897 camera. A control experiment was performed, following a previously described method, without immobilizing **Bio-NV** on a biotin micropatterned surface.

Hexapeptide NV and Cellular Microtubule Interaction Study by Confocal Microscopy. PC12 neural cells having cell density of 3000−5000 cells/coverslip were grown on a coverslip and harvested overnight. Then media was changed with the treatment solution containing 100 μM of **FITC-NV** peptide. After 16 h of incubation, complete media was aspirated, and the coverslip was washed with serum free media. Cells were fixed with 4% paraformaldehyde for 1 h and incubated with 0.2% triton-X and 5% BSA in PBS for 1 h. After a single wash with 1× PBS, cells were incubated with polyclonal anti-α-tubulin IgG antibody (Abcam) with dilution 1:300 for 2 h. Then cells were washed with PBS and incubated with secondary antibody (Cy3.5 preabsorbed goat anti-rabbit IgG; Abcam) having dilution 1:600 for 2 h. Cells were washed with 1× PBS followed by incubation with Hoechst 33258 from Calbiochem (1 μg/mL) for 30 min before imaging. Microscopy image was taken in a confocal microscope with a 60× objective (Olympus) and an Andor iXon3 897 EMCCD camera in 405, 488, and 561 nm wavelength laser lights.

Cell Culture. Rat pheochromocytoma cells (PC12) cells were cultured as described previously (Supporting Information) in RPMI medium supplemented with 10% heat-inactivated horse serum (HS) and 5% heat-inactivated fetal bovine serum. Neuronal differentiation of these cells was induced by NGF (100 ng/mL) in medium containing 1% horse serum for 6 days before the treatment, as previously described.

Cell Viability Assay. The cell viability was checked by the intact nuclear counting method. This assay was performed as described previously. In brief, a detergent containing the buffer that dissolved only the plasma membrane was added to the cells, the nuclear membrane thus remained intact. The intact nuclei were then counted on a hemocytometer under a light microscope. The number of live cells was expressed as percentage of the total cell population.

MD Simulation. For simulation study, a single peptide was kept at the center of a cubic box solvated by 2946 simple point charge (SPC) water models. One chlorine atom in the 4.5 nm cubic box was used to neutralize the system. Two random coil peptides, separated by 2.0 nm were solvated by 2944 simple point charge (SPC) water models. Two chlorine atoms were used to neutralize the system in 4.5 nm cubic box. For simulation study, GROMACS version 4.5.5 was used. Gromos 96 53a6 force field was applied for peptides. Periodic boundary conditions were applied in all three directions. Cutoff radii of 0.9 nm were set for electrostatic interactions and 1.4 nm for Lennard-Jones interactions. Long-range electrostatics interactions were tested using the particle-mesh Ewald (PME) method. Simulation was performed at a time step of 2 fs. The first phase involved simulation for 500 ps under a constant volume (NVT) ensemble. Using the V-rescale coupling method we coupled protein and nonprotein atoms to separate coupling baths, and temperature was maintained at 310 K. Following NVT equilibration, 1 ns of constant-pressure (NPT) equilibration was performed using the Parrinello−Rahman coupling method. Relaxation times of 1 and 0.1 ps were used for NPT and NVT, respectively. Then production run was performed for 100 ns. LINCS algorithm was used to constrain bond lengths. For four molecules, we used a similar method as described before, and details are described in Supporting Information.

Docking. Autodock-Vina software version 1.1.2 was used for blind docking. A 98 × 60 × 64 affinity grid box was centered on the receptor (1 JFF) for tubulin−**NV** peptide docking, and 40 × 26 × 54 affinity grids were centered on the receptor Alzheimer amyloid β peptide (PDB ID 1IYT) for Aβ−**NV** peptide docking interaction. The protein−peptide interaction was represented using a 2D interaction plot, which was plotted with the help of Ligplot (Supporting Information).

Data Analysis. Microscopic images were analyzed using ImageJ software.

■ ASSOCIATED CONTENT

Ⓢ Supporting Information

Additional methods, HPLC chromatogram of **NV** and **Biotin-NV**, MS data for **NV** and **Biotin-NV**, CD spectrum of NV, TEM images of NV, 2D representation of binding site structure

DOI: 10.1021/acschemneuro.5b00149
ACS Chem. Neurosci. 2015, 6, 1309−1316

with tubulin dimer, tubulin turbidity assay and microtubule assembly assay results, binding constant curve of tubulin and NV, images of NV interactions with Aβ, and MD simulation movies of two and four hexapeptides transforming to β-sheet structure. The Supporting Information is available free of charge on the ACS Publications website at DOI: 10.1021/acschemneuro.5b00149.

AUTHOR INFORMATION

Corresponding Author

*E-mail: sghosh@iicb.res.in.

Notes

The authors declare no competing financial interest.

ACKNOWLEDGMENTS

Authors wish to thank CSIR-IICB for Live Cell Imaging Facility and Prof. S. Verma, IIT Kanpur and Prof. Kankan Bhattacharyya, IACS Kolkata for suggestions and generous help. PK, SS, BJ, PM and AS thank CSIR, India. AB, SM and AA are thankful to UGC, India for their fellowship. DB thanks DST, India for Inspired fellowship. SG and SCB are supported by miND project grant (BSC0115) from CSIR, India. SG also thanks DST, India for Ramanujan fellowship.

REFERENCES

(1) Videnovic, A., Lazar, A. S., Barker, R. A., and Overeem, S. (2014) 'The clocks that time us'—circadian rhythms in neurodegenerative disorders. *Nat. Rev. Neurol. 10*, 683−693.

(2) Barrow, C. J., and Zagorski, M. G. (1991) Solution structures of beta peptide and its constituent fragments: relation to amyloid deposition. *Science 253*, 179−182.

(3) Masters, C. L., Simms, G., Weinman, N. A., Multhaup, G., McDonald, B. L., and Beyreuther, K. (1985) Amyloid plaque core protein in Alzheimer disease and Down syndrome. *Proc. Natl. Acad. Sci. U. S. A. 82*, 4245−4249.

(4) LaFerla, F. M., Green, K. N., and Oddo, S. (2007) Intracellular amyloid-beta in Alzheimer's disease. *Nat. Rev. Neurosci. 8*, 499−509.

(5) Borysov, S. I., Granic, A., Padmanabhan, J., Walczak, C. E., and Potter, H. (2011) Alzheimer Aβ disrupts the mitotic spindle and directly inhibits mitotic microtubule motors. *Cell Cycle 10*, 1397−1410.

(6) Saha, A., Mohapatra, S., Kurkute, P., Jana, B., Mondal, P., Bhunia, D., Ghosh, S., and Ghosh, S. (2015) Interaction of Aβ peptide with tubulin causes an inhibition of tubulin polymerization and the apoptotic death of cancer cells. *Chem. Commun. 51*, 2249−2252.

(7) Blanchard, B. J., Chen, A., Rozeboom, L. M., Stafford, K. A., Weigele, P., and Ingram, V. M. (2004) Efficient reversal of Alzheimer's disease fibril formation and elimination of neurotoxicity by a small molecule. *Proc. Natl. Acad. Sci. U. S. A. 101*, 14326−14332.

(8) Lorenzo, A., and Yankner, B. A. (1994) Beta-amyloid neurotoxicity requires fibril formation and is inhibited by congo red. *Proc. Natl. Acad. Sci. U. S. A. 91*, 12243−12247.

(9) Zhu, M., Rajamani, S., Kaylor, J., Han, S., Zhou, F., and Fink, A. L. (2004) The Flavonoid Baicalein Inhibits Fibrillation of α-Synuclein and Disaggregates Existing Fibrils. *J. Biol. Chem. 279*, 26846−26857.

(10) Heiser, V., Scherzinger, E., Boeddrich, A., Nordhoff, E., Lurz, R., Schugardt, N., Lehrach, H., and Wanker, E. E. (2000) Inhibition of huntingtin fibrillogenesis by specific antibodies and small molecules: Implications for Huntington's disease therapy. *Proc. Natl. Acad. Sci. U. S. A. 97*, 6739−6744.

(11) McGovern, S. L., Caselli, E., Grigorieff, N., and Shoichet, B. K. (2002) A common mechanism underlying promiscuous inhibitors from virtual and high-throughput screening. *J. Med. Chem. 45*, 1712−1722.

(12) Jouroukhin, Y., Ostritsky, R., Assaf, Y., Pelled, G., Giladi, E., and Gozes, I. (2013) NAP (davunetide) modifies disease progression in a mouse model of severe neurodegeneration: protection against impairments in axonal transport. *Neurobiol. Dis. 56*, 79−94.

(13) Biswas, A., Kurkute, P., Jana, B., Laskar, A., and Ghosh, S. (2014) An amyloid inhibitor octapeptide forms amyloid type fibrous aggregates and affects microtubule motility. *Chem. Commun. 50*, 2604−2607.

(14) Feng, B. Y., Toyama, B. H., Wille, H., Colby, D. W., Collins, S. R., May, B. C. H., Prusiner, S. B., Weissman, J., and Shoichet, B. K. (2008) Small-molecule aggregates inhibit amyloid polymerization. *Nat. Chem. Biol. 4*, 197−199.

(15) Chakraborti, S., Das, L., Kapoor, A. N., Dwivedi, V., Poddar, A., Chakraborti, G., Janik, M., Basu, G., Panda, D., Chakrabarti, P., Surolia, A., and Bhattacharyya, B. (2011) Curcumin recognizes a unique binding site of tubulin. *J. Med. Chem. 54*, 6183−6196.

(16) Bonne, D., Heusele, C., Simon, C., and Pantaloni, D. (1984) 4′,6-Diamidino-2-phenylindole, a fluorescent probe for tubulin and microtubules. *J. Biol. Chem. 260*, 2819−2825.

(17) Smith, C. D., and Zhang, X. (1996) Mechanism of Action of Cryptophycin. *J. Biol. Chem. 271*, 6192−6198.

(18) Khanna, S., Jana, B., Saha, A., Kurkute, P., Ghosh, S., and Verma, S. (2014) Targeting cytotoxicity and tubulin polymerization by metal−carbene complexes on a purine tautomer platform. *Dalton Trans. 43*, 9838−9842.

(19) Jana, B., Sarkar, J., Mondal, P., Barman, S., Mohapatra, S., Bhunia, D., Pradhan, K., Saha, A., Adak, A., Ghosh, S., and Ghosh, S. (2015) A short GC rich DNA derived from microbial origin targets tubulin/microtubule and induces apoptotic death of cancer cell. *Chem. Commun.*, DOI: 10.1039/C5CC03432A.

(20) Crescenzi, O., Tomaselli, S., Guerrini, R., Salvadori, S., D'Ursi, A. M., Temussi, P. A., and Picone, D. (2002) Solution structure of the alzheimer amyloid b-peptide (1−42) in an apolar microenvironment. *Eur. J. Biochem. 269*, 5642−5648.

(21) Gordon, D. J., Sciarretta, K. L., and Meredith, S. C. (2001) Inhibition of *beta*-Amyloid (40) Fibrillogenesis and disassembly of *beta*-amyloid (40) fibrils by short *beta*-amyloid congeners containing *N*-methyl amino acids at alternate residues. *Biochemistry 40*, 8237−8245.

(22) Bieler, S., and Soto, C. (2004) β-Sheet Breakers for Alzheimer's Disease Therapy. *Curr. Drug Targets 5*, 553−558.

(23) Lührs, T., Ritter, C., Adrian, M., Riek-Loher, D., Bohrmann, B., Döbeli, H., Schubert, D., and Riek, R. (2005) 3D structure of alzheimer's amyloid-beta (1− 42) fibrils. *Proc. Natl. Acad. Sci. U. S. A. 102*, 17342−17347.

(24) Sanphui, P., Pramanik, S. K., Chatterjee, N., Moorthi, P., Banerji, B., and Biswas, S. C. (2013) Efficacy of cyclin dependent kinase 4 inhibitors as potent neuroprotective agents against insults relevant to Alzheimer's disease. *PLoS One 8*, e78842.

(25) Matrone, C., Di Luzio, A., Meli, G., D'Aguanno, S., Severini, C., Ciotti, M. T., Cattaneo, A., and Calissano, P. (2008) Activation of the amyloidogenic route by NGF deprivation induces apoptotic death in PC12 cells. *J. Alzheimer's Dis. 13*, 81−96.

(26) Cattaneo, A., and Calissano, P. (2012) Nerve growth factor and Alzheimer's disease: new facts for an old hypothesis. *Mol. Neurobiol. 46*, 588−604.

(27) Greene, L. A., and Tischler, A. S. (1976) Establishment of a noradrenergic clonal line of rat adrenal pheochromocytoma cells which respond to nerve growth factor. *Proc. Natl. Acad. Sci. U. S. A. 73*, 2424−2428.

(28) Biswas, S. C., and Greene, L. A. (2002) Nerve growth factor (NGF) down-regulates the Bcl-2 homology 3 (BH3) domain-only protein Bim and suppresses its proapoptotic activity by phosphorylation. *J. Biol. Chem. 277*, 49511−49516.

(29) Xu, Z., Maroney, A. C., Dobrzanski, P., Kukekov, N. V., and Greene, L. A. (2001) The MLK family mediates c-Jun N-terminal kinase activation in neuronal apoptosis. *Mol. Cell. Biol. 21*, 4713−4724.

DOI: 10.1021/acschemneuro.5b00149
ACS Chem. Neurosci. 2015, 6, 1309−1316